

Observation of $\psi(3686) \rightarrow K^- \Lambda(1520) \bar{\Xi}^+ + \text{c.c.}$



The BESIII collaboration

E-mail: besiii-publications@ihep.ac.cn

ABSTRACT: Based on $(2712.4 \pm 14.3) \times 10^6$ $\psi(3686)$ events collected at the BESIII detector operating at the BEPCII collider, we present the first observation of the decay $\psi(3686) \rightarrow K^- \Lambda(1520) \bar{\Xi}^+ + \text{c.c.}$. The product branching fraction $\mathcal{B}[\psi(3686) \rightarrow K^- \Lambda(1520) \bar{\Xi}^+ + \text{c.c.}] \times \mathcal{B}[\Lambda(1520) \rightarrow p K^-]$ is measured to be $(9.47 \pm 0.75 \pm 0.97) \times 10^{-7}$, where the first uncertainty is statistical and the second systematic.

KEYWORDS: Branching fraction, e^+e^- Experiments, Quarkonium, QCD

ARXIV EPRINT: [2501.02594](https://arxiv.org/abs/2501.02594)

Contents

1	Introduction	1
2	BESIII detector and Monte Carlo simulation	2
3	Event selection	2
4	Background study	4
5	Intermediate state	5
6	Signal yield and branching fraction	5
7	Systematic uncertainty	7
8	Summary	9
	The BESIII collaboration	12

1 Introduction

The discovery of J/ψ and other charmonium states of $c\bar{c}$ played important roles in the development of the theory of the strong interaction in the Standard Model (SM) [1, 2]. These states can probe a wide range of energy scales in the Quantum Chromodynamics (QCD) from high-energy to low-energy regions, where the non-perturbative effects become dominant [3]. Experimental study on hadronic decays of charmonium states is a bridge between perturbative QCD and non-perturbative QCD. Many topics involving strong interaction can be investigated, such as color octet and singlet contributions, the violation of helicity conservation, and SU(3) flavor symmetry breaking effects [3, 4]. Since baryons represent the simplest system in which three colors of quarks neutralize into colorless objects with the essential non-Abelian character of QCD, a systematic study of baryon spectroscopy can provide critical insights into the nature of QCD in the confinement domain.

Compared to two-body final states, the theoretical calculation for three-body decays of charmonium states is more challenging. The decays of charmonium states into three-body final states are helpful in the search for excited baryon states and threshold enhancements, and numerous such decay modes have been studied recently [5]. However, the study of baryon spectroscopy remains incomplete, with many of the states predicted by SU(3) multiplets yet to be discovered or well-established. Most published measurements of $\psi(3686)$ decays involve zero or one strange quark [6]. The knowledge of excited baryon states with two strange quarks, i.e. Ξ^* hyperons, is particularly limited due to their small production rates and complicated decay topology. To date, only several states have been observed, and few of them have well-determined spin and parity. Further searches and detailed investigations into excited baryons are important to further understand the QCD mechanism.

In this paper, we report the first observation of the decay $\psi(3686) \rightarrow K^- \Lambda(1520) \bar{\Xi}^+ + \text{c.c.}$, and the measurement of the product branching fraction $\mathcal{B}[\psi(3686) \rightarrow K^- \Lambda(1520) \bar{\Xi}^+ + \text{c.c.}] \times \mathcal{B}[\Lambda(1520) \rightarrow pK^-]$, based on $(2712.4 \pm 14.3) \times 10^6$ $\psi(3686)$ events collected with the BESIII detector [7]. Throughout this paper, the charge conjugation decay mode is always implied.

2 BESIII detector and Monte Carlo simulation

The BESIII detector is a magnetic spectrometer [8, 9] located at the Beijing Electron Positron Collider (BEPCII) [10], which operates with a peak luminosity of $1.1 \times 10^{33} \text{ cm}^{-2} \text{ s}^{-1}$ in the center-of-mass (CM) energy range from 1.85 to 4.95 GeV. A helium-based multilayer drift chamber (MDC), a plastic scintillator time-of-flight system (TOF), and a CsI(Tl) electromagnetic calorimeter (EMC) compose the cylindrical core of the BESIII detector, and they are all enclosed in a superconducting solenoidal magnet providing a 1.0 T magnetic field. The solenoid is supported by an octagonal flux-return yoke with resistive plate counter muon identifier modules interleaved with steel. The acceptance of charged particles and photons is 93% over a 4π solid angle. The charged-particle momenta resolution at 1.0 GeV/ c is 0.5%, and the specific energy loss (dE/dx) resolution is 6% for the electrons from Bhabha scattering at 1 GeV. The EMC measures photon energies with a resolution of 2.5%(5%) at 1 GeV in the barrel (end-cap) region. The time resolution of the TOF barrel part is 68 ps, while that of the end-cap part is 110 ps. The end-cap TOF was upgraded in 2015 with multi-gap resistive plate chamber technology, providing a time resolution of 60 ps [11–13], which benefits 85% of the data used in this analysis.

Simulated samples produced with a GEANT4-based [14] Monte Carlo (MC) package, which includes the geometric description of the BESIII detector and the detector response, are used to determine detection efficiency and estimate backgrounds. The simulation models the beam energy spread and initial state radiation in the e^+e^- annihilations with the generator KKMC [15, 16]. The inclusive MC sample includes the production of the $\psi(3686)$ resonance, the initial-state radiation production of the J/ψ meson, and the continuum processes incorporated in KKMC [15, 16]. All particle decays are modelled with EVTGEN [17, 18] using branching fractions either taken from the Particle Data Group (PDG) [6], when available, or otherwise estimated with LUNDCHARM [19, 20] for the unknown ones. Final state radiation from charged final state particles is incorporated using PHOTOS [21]. To determine the detection efficiency, a signal MC sample of $\psi(3686) \rightarrow K^- \Lambda(1520) \bar{\Xi}^+, \bar{\Xi}^+ \rightarrow \bar{\Lambda} \pi^+, \bar{\Lambda} \rightarrow \bar{p} \pi^+$, and $\Lambda(1520) \rightarrow pK^-$ is generated uniformly in phase-space (PHSP). An inclusive $\psi(3686)$ MC sample, consisting of 2747×10^6 events, is used to estimate potential backgrounds. The data sample collected at a CM energy of 3.773 GeV, corresponding to an integrated luminosity of 2.93 fb^{-1} , is used to estimate the continuum background.

3 Event selection

The cascade decay of interest is $\psi(3686) \rightarrow K^- \Lambda(1520) \bar{\Xi}^+, \Lambda(1520) \rightarrow pK^-$, where $\bar{\Xi}^+ \rightarrow \bar{\Lambda} \pi^+$, and $\bar{\Lambda} \rightarrow \bar{p} \pi^+$. In track-level selection, at least six charged tracks are reconstructed within the polar angle (θ) range of $|\cos \theta| < 0.93$, where θ is defined with respect to the z -axis, which is the symmetry axis of the MDC. Since the bachelor kaon and the two tracks

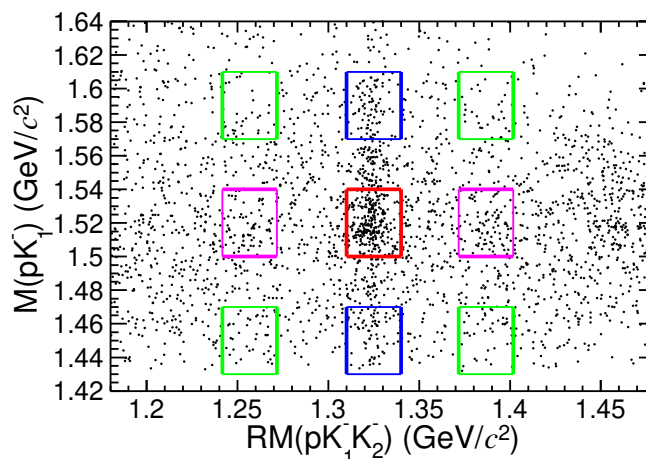


Figure 1. The distributions of $RM(pK_1^- K_2^-)$ versus $M(pK_1^-)$ for data events.

from $\Lambda(1520)$ decay have no secondary vertex, we further require at least three tracks to originate from the interaction point (IP), i.e. $V_r < 1$ cm, $|V_z| < 10$ cm, where V_r and V_z are the closest approaches of the tracks to the IP in transverse plane and in z coordinate respectively. For each charged track, particle identification (PID) is performed. At least six charged particles, $p\bar{p}K^-K^-\pi^+\pi^+$, are identified by combining measurements of the dE/dx in the MDC and the flight time in the TOF to form PID likelihoods for each particle hypothesis. If there are multiple combinations of $p\bar{p}K^-K^-\pi^+\pi^+$, the combination with the largest sum of PID likelihoods is kept for further analysis. The Ξ^+ is tagged by the recoil mass of proton and two kaons, $RM(pK_1^- K_2^-)$. Here (and elsewhere), K_1^- denotes the kaon from $\Lambda(1520)$ decay, while K_2^- denotes the bachelor. The K_1 is assigned by requiring its invariant mass $M(pK_1^-)$ to be closer to the mass of $\Lambda(1520)$.

Figure 1 shows the 2D distribution of the recoil mass of $pK_1^- K_2^-$ versus the mass of pK_1^- for data events, where the red box denotes the signal region of $\Xi^+ - \Lambda(1520)$, while the eight boxes with the same area around signal region are taken as the 2D sideband. Figure 2(a) shows the $RM(pK_1^- K_2^-)$ distribution of the survived candidate events. A clear Ξ^+ signal is observed. We define the recoil mass range $1.31 \text{ GeV}/c^2 < RM(pK_1^- K_2^-) < 1.34 \text{ GeV}/c^2$ as the Ξ^+ signal region, while the sideband regions are defined as $1.242 \text{ GeV}/c^2 < RM(pK_1^- K_2^-) < 1.272 \text{ GeV}/c^2$ and $1.372 \text{ GeV}/c^2 < RM(pK_1^- K_2^-) < 1.402 \text{ GeV}/c^2$. Figure 2(b) shows the $M(pK_1^-)$ distribution of the events in the Ξ^+ signal and sideband regions, and a clear $\Lambda(1520)$ signal is observed, while no obvious peaking background is found in the Ξ^+ sideband events. The $\Lambda(1520)$ signal region is defined as $1.50 \text{ GeV}/c^2 < M(pK_1^-) < 1.54 \text{ GeV}/c^2$, while the sideband regions are defined as $1.43 \text{ GeV}/c^2 < M(pK_1^-) < 1.47 \text{ GeV}/c^2$ and $1.57 \text{ GeV}/c^2 < M(pK_1^-) < 1.61 \text{ GeV}/c^2$. The normalization factor (f_{sideband}) of the Ξ^+ signal over the sideband regions is determined to be 0.47 ± 0.01 (0.49 ± 0.01 for c.c. mode) according to the areas of the fitted background function between signal and sideband regions, as shown in figure 2(a). This factor is then used to normalize the number of non- Ξ^+ background events estimated from the sideband regions.

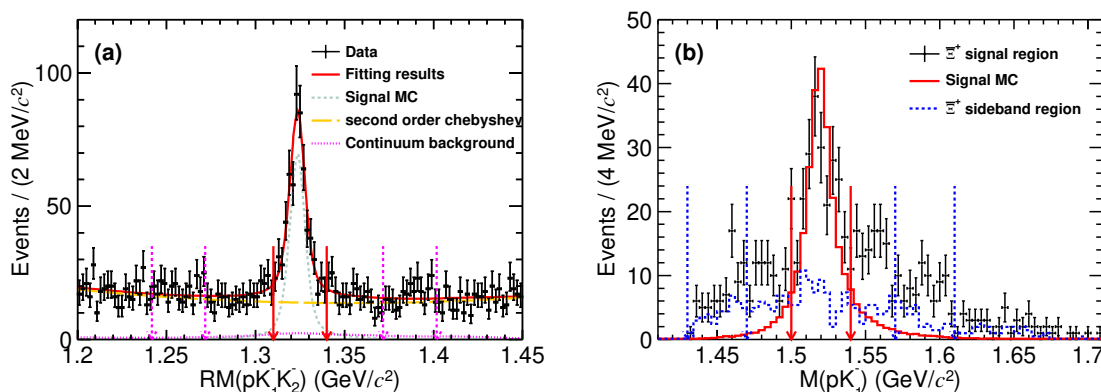


Figure 2. (a) The distribution of $RM(pK_1^- K_2^-)$ from data. The red solid and purple dashed arrows denote the Ξ^+ signal and sideband regions, respectively; (b) The distribution of $M(pK_1^-)$ in the Ξ^+ signal and sideband regions from both data and MC simulation, where the normalization factor has been applied to the sideband distribution. The red solid and blue dashed arrows denote the $\Lambda(1520)$ signal and sideband regions, respectively.

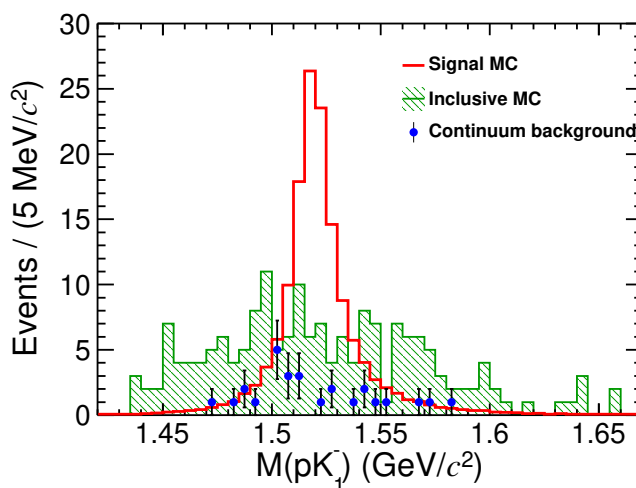


Figure 3. The distributions of $M(pK_1^-)$ from the inclusive MC sample and the continuum data. The red solid line denotes the signal MC. The green-shaded histogram denotes the inclusive MC. The dots with error bars represent the continuum background.

4 Background study

The inclusive MC sample is used to investigate the potential backgrounds. Figure 3 shows the distribution of the invariant mass of pK_1^- for the accepted candidate events from simulated signal and background samples. Additionally, the events selected from the sample collected at $\sqrt{s} = 3.773$ GeV are analyzed to investigate the continuum production. No significant peaking background is found in either the inclusive MC sample or the continuum sample.

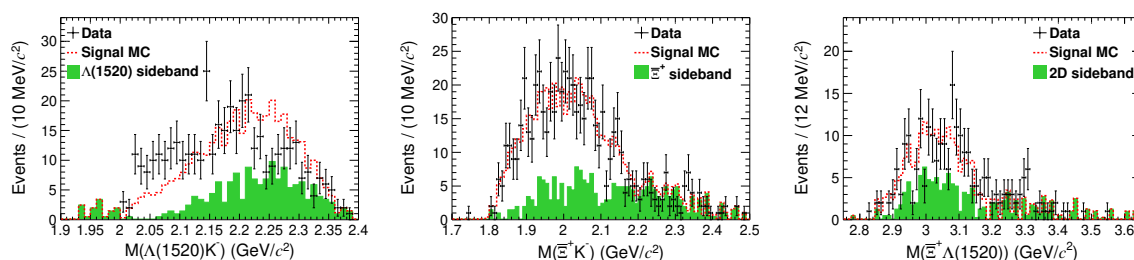


Figure 4. (a,b,c) The distributions of $M(\Lambda(1520)K^-)$, $M(\bar{\Xi}^+K^-)$, and $M(\bar{\Xi}^+\Lambda(1520))$ for data and signal MC events.

5 Intermediate state

To search for the potential intermediate states, we investigate the invariant mass spectra for all two-body combinations with the events in the $\bar{\Xi}^+$ signal region ($1.31 \text{ GeV}/c^2 < RM(pK_1^-K_2^-) < 1.34 \text{ GeV}/c^2$) or $\Lambda(1520)$ signal region ($1.50 \text{ GeV}/c^2 < M(pK_1^-) < 1.54 \text{ GeV}/c^2$). Figure 4 shows the distributions of $M(\Lambda(1520)K^-)$, $M(\bar{\Xi}^+K^-)$, and $M(\bar{\Xi}^+\Lambda(1520))$ for data and MC events generated with PHSP model, where the contributions from the normalized sideband have been added to MC sample. No obvious intermediate structure is observed in each distribution.

6 Signal yield and branching fraction

In investigating the intermediate states, we require one entry per event, which is likely to distort the background shape. To avoid this issue, the signal yield for $\psi(3686) \rightarrow K^-\Lambda(1520)\bar{\Xi}^+$, $\Lambda(1520) \rightarrow pK^-$, is obtained by performing an unbinned maximum likelihood fit to the combined $M(pK_1^-)$ and $M(pK_2^-)$ distributions with dual entries per event. The signal shape is described by the signal MC shape convolved with a Gaussian function which accounts for the difference in mass and mass resolution between data and MC simulation. The parameters of this Gaussian function are free to float in the fit.

The background components consist of the non- $\bar{\Xi}^+$, non- $\Lambda(1520)$, and continuum backgrounds. The shape and yield of the non- $\bar{\Xi}^+$ background is fixed in the fit according to the $\bar{\Xi}^+$ data sidebands after smoothing and normalization. The non- $\Lambda(1520)$ background from the four-body process ($\psi(3686) \rightarrow pK^-K^-\bar{\Xi}^+$) is described by the MC-simulated shape with its yield floating in the fit. The shape of the continuum background is taken from the data distribution at $\sqrt{s} = 3.773 \text{ GeV}$ as described in section 4. To account for the difference of the production cross sections and integrated luminosities between the two energies, the continuum background yield is scaled by a factor f_c calculated as

$$f_c = \frac{\mathcal{L}_{3.686}}{\mathcal{L}_{3.773}} \times \frac{\sigma_{3.686}}{\sigma_{3.773}}, \quad (6.1)$$

where $\mathcal{L}_{3.686} = 3877.05 \text{ pb}^{-1}$ and $\mathcal{L}_{3.773} = 2931.8 \text{ pb}^{-1}$ are the integrated luminosities at 3.686 GeV and 3.773 GeV, respectively; σ denotes the production cross section, which is assumed to be proportional to $1/s$. The value of f_c is determined to be 1.386.

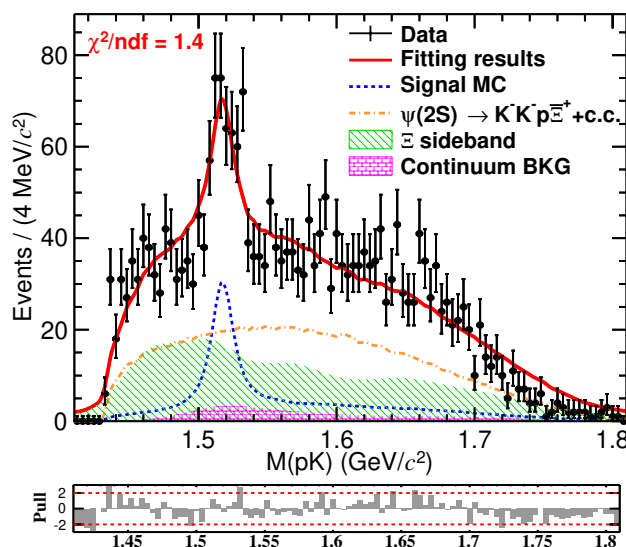


Figure 5. Fit to the M_{pK} distribution of the two charge conjugate signal modes. The dots with error bars represent the data sample events. The red solid line represents the fitting results. The blue dashed line represents the signal. The orange, green, and purple dashed lines denote the backgrounds from the non- $\Lambda(1520)$, non- Ξ , and continuum processes, respectively.

We fit to the dataset of the two charge conjugate channels together, which is taken as the nominal result. The goodness of the fit is $\chi^2/ndf = 108/76$, and the statistical significance of signal is 6.9σ . The significance is determined by comparing the likelihood difference with or without including $\Lambda(1520)$ signal contribution, and taking into account the change in the number of degrees of freedom [22]. Figure 5 shows the fit result for the sum of two charge conjugate channels, and the fitted number of $\Lambda(1520)$ signal is $190 \pm 15_{\text{stat.}}$, where the uncertainty is statistical. The nominal detection efficiency for the $\psi(3686) \rightarrow K^- \Lambda(1520) \bar{\Xi}^+ + \text{c.c.}$ channel is 11.55%, which is obtained as the average of the detection efficiencies of the two charge conjugate channels.

The product branching fraction $\mathcal{B}[\psi(3686) \rightarrow K^- \Lambda(1520) \bar{\Xi}^+ + \text{c.c.}] \times \mathcal{B}[\Lambda(1520) \rightarrow pK^-]$ is calculated via

$$\begin{aligned} & \mathcal{B}[\psi(3686) \rightarrow K^- \Lambda(1520) \bar{\Xi}^+ + \text{c.c.}] \times \mathcal{B}[\Lambda(1520) \rightarrow pK^-] \\ &= \frac{N^{\text{obs}}}{N_{\psi(3686)} \mathcal{B}(\bar{\Xi}^+ \rightarrow \bar{\Lambda} \pi^+) \mathcal{B}(\bar{\Lambda} \rightarrow \bar{p} \pi^+) \epsilon}, \end{aligned} \quad (6.2)$$

where N^{obs} represents the number of observed signal events; $N_{\psi(3686)}$ represents the total number of $\psi(3686)$ events in data; $\mathcal{B}(\bar{\Xi}^+ \rightarrow \bar{\Lambda} \pi^+)$ and $\mathcal{B}(\bar{\Lambda} \rightarrow \bar{p} \pi^+)$ denote the branching fractions of $\bar{\Xi}^+ \rightarrow \bar{\Lambda} \pi^+$ and $\bar{\Lambda} \rightarrow \bar{p} \pi^+$, respectively, which are taken from PDG [6]; ϵ is the detection efficiency. Finally, the product branching fraction $\mathcal{B}[\psi(3686) \rightarrow K^- \Lambda(1520) \bar{\Xi}^+ + \text{c.c.}] \times \mathcal{B}[\Lambda(1520) \rightarrow pK^-]$ is measured to be $(9.47 \pm 0.75) \times 10^{-7}$, where the uncertainty is statistical only.

7 Systematic uncertainty

The systematic uncertainties in the branching fraction measurement are from the tracking efficiency, PID efficiency, signal shape, non- $\Lambda(1520)$ background, continuum background, Ξ mass window, Ξ sideband, MC imperfection, MC statistics, total number of $\psi(3686)$ events, and the cited branching fractions. The details are discussed below:

- Tracking efficiency. Based on the control samples $J/\psi \rightarrow K_S^0 K^\pm \pi^\mp$, and $J/\psi \rightarrow p\bar{p}\pi^+\pi^-$, the relative difference of the MDC tracking efficiencies between data and MC simulation has been estimated in the polar angle and momentum distributions. The uncertainties related to tracking for kaons, pions, protons, and antiprotons are estimated to be 0.7%, 1.6%, 0.6%, and 0.5%, respectively.
- PID efficiency. Based on the control samples $J/\psi \rightarrow K_S^0 K^\pm \pi^\mp$, and $J/\psi \rightarrow p\bar{p}\pi^+\pi^-$, the relative difference of the PID efficiencies between data and MC simulation has been estimated in the polar angle and momentum distributions. The uncertainties related to PID for kaons, pions, protons, and antiprotons are estimated to be 0.1%, 1.0%, 0.3%, 0.5%, respectively.
- Signal shape. The uncertainty related to the signal shape is estimated by replacing the MC-simulated shape with an alternative one, in which a Breit-Wigner function convolved with a double Gaussian is used to model the $\Lambda(1520)$ and the MC simulated shape is utilized to describe the wrong pK^- combination, with the yield ratio of these two components fixed to one. The difference of the fitted signal yield with the nominal one, 5.0%, is assigned as the uncertainty.
- Non- $\Lambda(1520)$ background. The uncertainty due to the non- $\Lambda(1520)$ background is estimated by replacing the background shape from the MC-simulated shape to a seventh-order polynomial multiplied by an Argus function [23]. The difference of resulted signal yield with the nominal one is taken as the uncertainty, which is 4.1%.
- Continuum background. The uncertainty due to the event number of continuum background is estimated to be 1.0%, by varying the continuum background yield in the fit by one standard deviation, assuming it follows a Poisson distribution. The uncertainty caused by the continuum background shape is estimated to be 1.2%, by adjusting the bandwidth scale factor from 0.1 to 5.0, which controls the smoothness of the Kernel Estimation [24]. By combining them together, the uncertainty related to the continuum background is taken as 1.6%.
- Ξ mass window. The uncertainty due to the requirement of Ξ mass window is estimated with the control sample $J/\psi \rightarrow \Xi^- \bar{\Xi}^+$. The relative efficiency of this requirement is calculated as $\frac{N_{\text{with}}}{N_{\text{without}}}$, where N_{with} and N_{without} denote the number of events obtained with and without the Ξ mass window requirement. The difference of this efficiency between data and MC, 5.1%, is taken as the corresponding uncertainty.
- Ξ sideband. The uncertainty caused by Ξ sideband is estimated by varying the Ξ sideband region from $[m_\Xi - 0.08, m_\Xi - 0.05] \cup [m_\Xi + 0.05, m_\Xi + 0.08]$ to $[m_\Xi - 0.085, m_\Xi - 0.055] \cup [m_\Xi + 0.055, m_\Xi + 0.085]$ GeV/ c^2 . The resulted uncertainty is negligible.

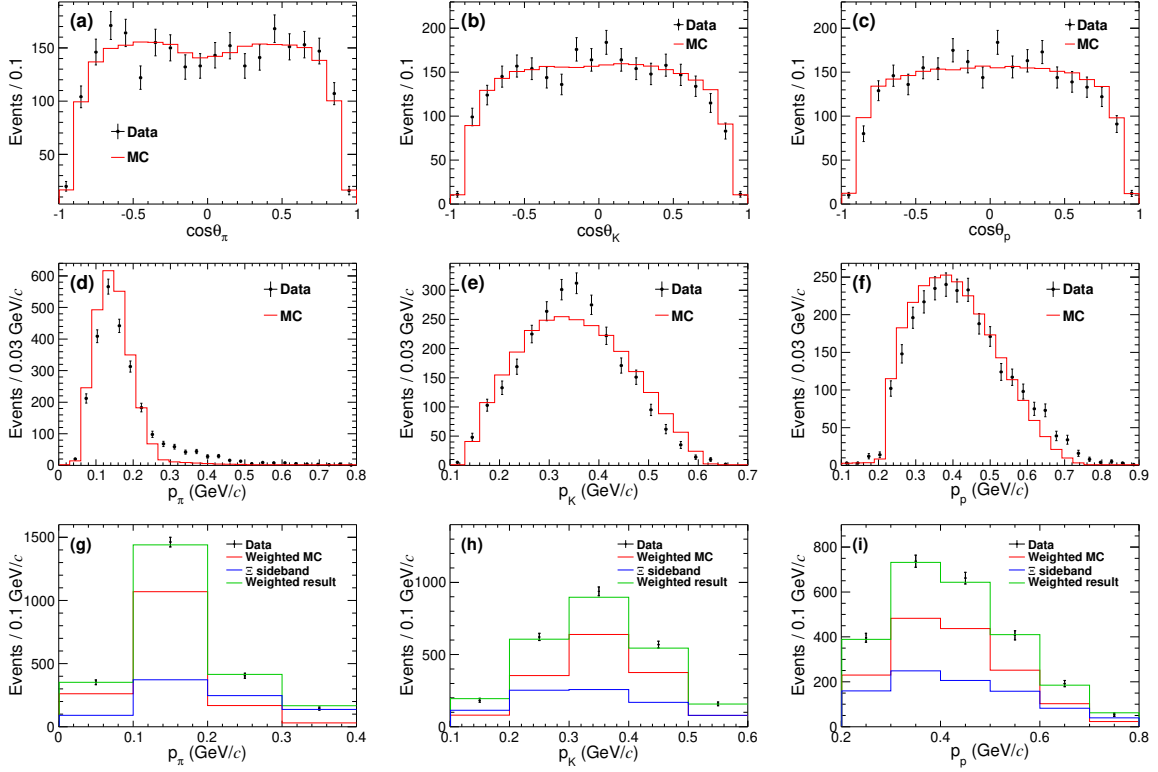


Figure 6. The one-dimensional comparisons of $\cos\theta$ (a,b,c), and momentum (d,e,f) distributions of pions, kaons, protons, and antiprotons from data and signal MC samples. Projections of the weighted result based on the three-dimensional distribution of momentum is also shown (g,h,i), where the dots with error bars represent the data; the red, and blue solid lines denote the weighted signal MC, and Ξ sideband respectively and the green solid line is the sum of the two.

- MC imperfection. We check the $\cos\theta$ and momentum distributions of pions, kaons, protons, and antiprotons from both data and signal MC samples, which are shown in figure 6. There are some differences in the momentum distributions. To estimate the uncertainty caused by MC imperfection, the efficiency is weighted according to the data momentum distributions where the normalized backgrounds from the Ξ sideband have been subtracted. The weighted efficiency is calculated via

$$\bar{\epsilon} = \frac{\sum_{i,j,k} n_{i,j,k}^{\text{MC}} \cdot \epsilon_{i,j,k}}{\sum_{i,j,k} n_{i,j,k}^{\text{truth}} \cdot \epsilon_{i,j,k}}, \quad (7.1)$$

where

$$\epsilon_{i,j,k} = \begin{cases} (n_{i,j,k}^{\text{data}} - n_{i,j,k}^{\text{sideband}} \cdot f_{\text{sideband}}) / n_{i,j,k}^{\text{MC}}, & n_{i,j,k}^{\text{MC}} \neq 0 \\ 1, & n_{i,j,k}^{\text{MC}} = 0. \end{cases} \quad (7.2)$$

Here, $n_{i,j,k}^{\text{MC}}$, $n_{i,j,k}^{\text{truth}}$, $n_{i,j,k}^{\text{data}}$, and $n_{i,j,k}^{\text{sideband}}$ refer to the numbers of events in the (i, j, k) -th bin of MC, MC truth, data, and Ξ sideband samples. The associated uncertainty is determined to be 4.1%.

- MC statistics. The uncertainty is negligible due to the large generated MC sample.

Source	Uncertainty (%)
Tracking	3.4
PID	1.9
Signal shape	5.0
Non- $\Lambda(1520)$ background	4.1
Continuum background	1.6
Ξ mass window	5.1
Ξ sideband	Negligible
MC imperfection	4.1
MC statistics	Negligible
Total number of $\psi(3686)$ events	0.5
Quoted branching fractions	0.8
Total	10.2

Table 1. Systematic uncertainties in the branching fraction measurement.

- Total number of $\psi(3686)$ events. The uncertainty of the total number of $\psi(3686)$ events is 0.5% [7].
- The quoted branching fractions. The uncertainty due to the quoted branching fraction $\Lambda \rightarrow p\pi^+$, is 0.8% according to the PDG [6]. The uncertainty from the branching fraction of $\Xi^- \rightarrow \Lambda\pi^-$ is negligible.

All of the systematic uncertainties are summarized in table 1. Adding them in quadrature results in a total systematic uncertainty of 10.2% in the branching fraction measurement.

Additionally, the signal significance is updated to be 5.0σ after considering the uncertainties related to the signal shape, non- $\Lambda(1520)$ background, continuum background, and Ξ mass window.

8 Summary

In summary, using a sample of 2.7 billion $\psi(3686)$ events collected with the BESIII detector, the decay $\psi(3686) \rightarrow K^- \Lambda(1520) \bar{\Xi}^+ + \text{c.c.}$ is observed for the first time with a significance of 5.0 standard deviations, after considering both statistical and systematic uncertainties. The product branching fraction $\mathcal{B}[\psi(3686) \rightarrow K^- \Lambda(1520) \bar{\Xi}^+ + \text{c.c.}] \times \mathcal{B}[\Lambda(1520) \rightarrow pK^-]$ is measured to be $(9.47 \pm 0.75 \pm 0.97) \times 10^{-7}$, where the first uncertainty is statistical and the second systematic. With the current sample size, no evidence of excited baryon state or threshold enhancement is observed. A larger $\psi(3686)$ data sample may help to study the dynamics of this decay.

Acknowledgments

The BESIII Collaboration thanks the staff of BEPCII and the IHEP computing center for their strong support. This work is supported in part by National Key R&D Program of China under Contracts Nos. 2020YFA0406300, 2020YFA0406400, 2023YFA1606000; National Natural

Science Foundation of China (NSFC) under Contracts Nos. 11635010, 11735014, 11935015, 11935016, 11935018, 12025502, 12035009, 12035013, 12061131003, 12192260, 12192261, 12192262, 12192263, 12192264, 12192265, 12221005, 12225509, 12235017, 12361141819, 12275067, 12475197; the Science and Technology R&D Program Joint Fund Project of Henan Province (Grant No. 225200810030); the Science and Technology Innovation Leading Talent Support Program of Henan Province; the Chinese Academy of Sciences (CAS) Large-Scale Scientific Facility Program; the CAS Center for Excellence in Particle Physics (CCEPP); Joint Large-Scale Scientific Facility Funds of the NSFC and CAS under Contract No. U1832207; 100 Talents Program of CAS; The Institute of Nuclear and Particle Physics (INPAC) and Shanghai Key Laboratory for Particle Physics and Cosmology; German Research Foundation DFG under Contracts Nos. FOR5327, GRK 2149; Istituto Nazionale di Fisica Nucleare, Italy; Knut and Alice Wallenberg Foundation under Contracts Nos. 2021.0174, 2021.0299; Ministry of Development of Turkey under Contract No. DPT2006K-120470; National Research Foundation of Korea under Contract No. NRF-2022R1A2C1092335; National Science and Technology fund of Mongolia; National Science Research and Innovation Fund (NSRF) via the Program Management Unit for Human Resources & Institutional Development, Research and Innovation of Thailand under Contracts Nos. B16F640076, B50G670107; Polish National Science Centre under Contract No. 2019/35/O/ST2/02907; Swedish Research Council under Contract No. 2019.04595; The Swedish Foundation for International Cooperation in Research and Higher Education under Contract No. CH2018-7756; U. S. Department of Energy under Contract No. DE-FG02-05ER41374.

Data Availability Statement. This article has no associated data or the data will not be deposited.

Code Availability Statement. This article has no associated code or the code will not be deposited.

Open Access. This article is distributed under the terms of the Creative Commons Attribution License ([CC-BY4.0](https://creativecommons.org/licenses/by/4.0/)), which permits any use, distribution and reproduction in any medium, provided the original author(s) and source are credited.

References

- [1] E598 collaboration, *Experimental Observation of a Heavy Particle J*, *Phys. Rev. Lett.* **33** (1974) 1404 [[INSPIRE](#)].
- [2] SLAC-SP-017 collaboration, *Discovery of a Narrow Resonance in e^+e^- Annihilation*, *Phys. Rev. Lett.* **33** (1974) 1406 [[INSPIRE](#)].
- [3] D.M. Asner et al., *Physics at BES-III*, *Int. J. Mod. Phys. A* **24** (2009) S1 [[arXiv:0809.1869](#)] [[INSPIRE](#)].
- [4] A. Rybicki, *Hadronic interactions at the CERN SPS: Resonance decays versus parton dynamics*, *Int. J. Mod. Phys. A* **24** (2009) 385 [[INSPIRE](#)].
- [5] BESIII collaboration, *Observation of $\psi(3686) \rightarrow \Omega^- K^+ \Xi^0 + c.c.$* , *JHEP* **04** (2024) 013 [[arXiv:2401.08252](#)] [[INSPIRE](#)].

- [6] PARTICLE DATA GROUP collaboration, *Review of particle physics*, *Phys. Rev. D* **110** (2024) 030001 [INSPIRE].
- [7] BESIII collaboration, *Determination of the number of $\psi(3686)$ events taken at BESIII**, *Chin. Phys. C* **48** (2024) 093001 [arXiv:2403.06766] [INSPIRE].
- [8] BESIII collaboration, *Design and Construction of the BESIII Detector*, *Nucl. Instrum. Meth. A* **614** (2010) 345 [arXiv:0911.4960] [INSPIRE].
- [9] BESIII collaboration, *Future Physics Programme of BESIII*, *Chin. Phys. C* **44** (2020) 040001 [arXiv:1912.05983] [INSPIRE].
- [10] C. Yu et al., *BEPCII Performance and Beam Dynamics Studies on Luminosity*, in the proceedings of the *7th International Particle Accelerator Conference (IPAC'16)*, Busan, South Korea (2016) [DOI:10.18429/JACoW-IPAC2016-TUYA01] [INSPIRE].
- [11] X. Li et al., *Study of MRPC technology for BESIII endcap-TOF upgrade*, *Radiat. Detect. Technol. Methods* **1** (2017) 13 [INSPIRE].
- [12] Y.-X. Guo et al., *The study of time calibration for upgraded end cap TOF of BESIII*, *Radiat. Detect. Technol. Methods* **1** (2017) 15 [INSPIRE].
- [13] P. Cao et al., *Design and construction of the new BESIII endcap Time-of-Flight system with MRPC Technology*, *Nucl. Instrum. Meth. A* **953** (2020) 163053 [INSPIRE].
- [14] GEANT4 collaboration, *GEANT4 — A Simulation Toolkit*, *Nucl. Instrum. Meth. A* **506** (2003) 250 [INSPIRE].
- [15] S. Jadach, B.F.L. Ward and Z. Was, *Coherent exclusive exponentiation for precision Monte Carlo calculations*, *Phys. Rev. D* **63** (2001) 113009 [hep-ph/0006359] [INSPIRE].
- [16] S. Jadach, B.F.L. Ward and Z. Was, *The Precision Monte Carlo event generator K K for two fermion final states in e^+e^- collisions*, *Comput. Phys. Commun.* **130** (2000) 260 [hep-ph/9912214] [INSPIRE].
- [17] D.J. Lange, *The EvtGen particle decay simulation package*, *Nucl. Instrum. Meth. A* **462** (2001) 152 [INSPIRE].
- [18] R.-G. Ping, *Event generators at BESIII*, *Chin. Phys. C* **32** (2008) 599 [INSPIRE].
- [19] J.C. Chen et al., *Event generator for J/ψ and $\psi(2S)$ decay*, *Phys. Rev. D* **62** (2000) 034003 [INSPIRE].
- [20] R.-L. Yang, R.-G. Ping and H. Chen, *Tuning and Validation of the Lundcharm Model with J/ψ Decays*, *Chin. Phys. Lett.* **31** (2014) 061301 [INSPIRE].
- [21] E. Richter-Was, *QED bremsstrahlung in semileptonic B and leptonic τ decays*, *Phys. Lett. B* **303** (1993) 163 [INSPIRE].
- [22] S.S. Wilks, *The Large-Sample Distribution of the Likelihood Ratio for Testing Composite Hypotheses*, *Annals Math. Statist.* **9** (1938) 60 [INSPIRE].
- [23] ARGUS collaboration, *Search for Hadronic $b \rightarrow u$ Decays*, *Phys. Lett. B* **241** (1990) 278 [INSPIRE].
- [24] K.S. Cranmer, *Kernel estimation in high-energy physics*, *Comput. Phys. Commun.* **136** (2001) 198 [hep-ex/0011057] [INSPIRE].

The BESIII collaboration

M. Ablikim¹, M.N. Achasov^{4,c}, P. Adlarson⁷⁶, O. Afedulidis³, X.C. Ai⁸¹, R. Aliberti³⁵,
A. Amoroso^{75A,75C}, Q. An^{72,58,a}, Y. Bai⁵⁷, O. Bakina³⁶, I. Balossino^{29A}, Y. Ban^{46,h}, H.-R. Bao⁶⁴,
V. Batozskaya^{1,44}, K. Begzsuren³², N. Berger³⁵, M. Berlowski⁴⁴, M. Bertani^{28A}, D. Bettoni^{29A},
F. Bianchi^{75A,75C}, E. Bianco^{75A,75C}, A. Bortone^{75A,75C}, I. Boyko³⁶, R.A. Briere⁵, A. Brueggemann⁶⁹,
H. Cai⁷⁷, X. Cai^{1,58}, A. Calcaterra^{28A}, G.F. Cao^{1,64}, N. Cao^{1,64}, S.A. Cetin^{62A}, X.Y. Chai^{46,h},
J.F. Chang^{1,58}, G.R. Che⁴³, Y.Z. Che^{1,58,64}, G. Chelkov^{36,b}, C. Chen⁴³, C.H. Chen⁹, Chao Chen⁵⁵,
G. Chen¹, H.S. Chen^{1,64}, H.Y. Chen²⁰, M.L. Chen^{1,58,64}, S.J. Chen⁴², S.L. Chen⁴⁵, S.M. Chen⁶¹,
T. Chen^{1,64}, X.R. Chen^{31,64}, X.T. Chen^{1,64}, Y.B. Chen^{1,58}, Y.Q. Chen³⁴, Z.J. Chen^{25,i}, S.K. Choi¹⁰,
G. Cibinetto^{29A}, F. Cossio^{75C}, J.J. Cui⁵⁰, H.L. Dai^{1,58}, J.P. Dai⁷⁹, A. Dbeyssi¹⁸, R. E. de Boer³,
D. Dedovich³⁶, C.Q. Deng⁷³, Z.Y. Deng¹, A. Denig³⁵, I. Denysenko³⁶, M. Destefanis^{75A,75C},
F. De Mori^{75A,75C}, B. Ding^{67,1}, X.X. Ding^{46,h}, Y. Ding³⁴, Y. Ding⁴⁰, J. Dong^{1,58}, L.Y. Dong^{1,64},
M.Y. Dong^{1,58,64}, X. Dong⁷⁷, M.C. Du¹, S.X. Du⁸¹, Y.Y. Duan⁵⁵, Z.H. Duan⁴², P. Egorov^{36,b},
G.F. Fan⁴², J.J. Fan¹⁹, Y.H. Fan⁴⁵, J. Fang^{1,58}, J. Fang⁵⁹, S.S. Fang^{1,64}, W.X. Fang¹, Y.Q. Fang^{1,58},
R. Farinelli^{29A}, L. Fava^{75B,75C}, F. Feldbauer³, G. Felici^{28A}, C.Q. Feng^{72,58}, J.H. Feng⁵⁹,
Y.T. Feng^{72,58}, M. Fritsch³, C.D. Fu¹, J.L. Fu⁶⁴, Y.W. Fu^{1,64}, H. Gao⁶⁴, X.B. Gao⁴¹, Y.N. Gao¹⁹,
Y.N. Gao^{46,h}, Yang Gao^{72,58}, S. Garbolino^{75C}, I. Garzia^{29A,29B}, P.T. Ge¹⁹, Z.W. Ge⁴², C. Geng⁵⁹,
E.M. Gersabeck⁶⁸, A. Gilman⁷⁰, K. Goetzen¹³, L. Gong⁴⁰, W.X. Gong^{1,58}, W. Gradl³⁵,
S. Gramigna^{29A,29B}, M. Greco^{75A,75C}, M.H. Gu^{1,58}, Y.T. Gu¹⁵, C.Y. Guan^{1,64}, A.Q. Guo^{31,64},
L.B. Guo⁴¹, M.J. Guo⁵⁰, R.P. Guo⁴⁹, Y.P. Guo^{12,g}, A. Guskov^{36,b}, J. Gutierrez²⁷, K.L. Han⁶⁴,
T.T. Han¹, F. Hanisch³, X.Q. Hao¹⁹, F.A. Harris⁶⁶, K.K. He⁵⁵, K.L. He^{1,64}, F.H. Heinsius³,
C.H. Heinz³⁵, Y.K. Heng^{1,58,64}, C. Herold⁶⁰, T. Holtmann³, P.C. Hong³⁴, G.Y. Hou^{1,64}, X.T. Hou^{1,64},
Y.R. Hou⁶⁴, Z.L. Hou¹, B.Y. Hu⁵⁹, H.M. Hu^{1,64}, J.F. Hu^{56,j}, Q.P. Hu^{72,58}, S.L. Hu^{12,g}, T. Hu^{1,58,64},
Y. Hu¹, G.S. Huang^{72,58}, K.X. Huang⁵⁹, L.Q. Huang^{31,64}, P. Huang⁴², X.T. Huang⁵⁰, Y.P. Huang¹,
Y.S. Huang⁵⁹, T. Hussain⁷⁴, F. Hölzken³, N. Hüsken³⁵, N. in der Wiesche⁶⁹, J. Jackson²⁷,
S. Janchiv³², Q. Ji¹, Q.P. Ji¹⁹, W. Ji^{1,64}, X.B. Ji^{1,64}, X.L. Ji^{1,58}, Y.Y. Ji⁵⁰, X.Q. Jia⁵⁰, Z.K. Jia^{72,58},
D. Jiang^{1,64}, H.B. Jiang⁷⁷, P.C. Jiang^{46,h}, S.S. Jiang³⁹, T.J. Jiang¹⁶, X.S. Jiang^{1,58,64}, Y. Jiang⁶⁴,
J.B. Jiao⁵⁰, J.K. Jiao³⁴, Z. Jiao²³, S. Jin⁴², Y. Jin⁶⁷, M.Q. Jing^{1,64}, X.M. Jing⁶⁴, T. Johansson⁷⁶,
S. Kabana³³, N. Kalantar-Nayestanaki⁶⁵, X.L. Kang⁹, X.S. Kang⁴⁰, M. Kavatsyuk⁶⁵, B.C. Ke⁸¹,
V. Khachatryan²⁷, A. Khoukaz⁶⁹, R. Kiuchi¹, O.B. Kolcu^{62A}, B. Kopf³, M. Kuessner³, X. Kui^{1,64},
N. Kumar²⁶, A. Kupsc^{44,76}, W. Kühn³⁷, W.N. Lan¹⁹, T.T. Lei^{72,58}, Z.H. Lei^{72,58}, M. Lellmann³⁵,
T. Lenz³⁵, C. Li⁴⁷, C. Li⁴³, C.H. Li³⁹, Cheng Li^{72,58}, D.M. Li⁸¹, F. Li^{1,58}, G. Li¹, H.B. Li^{1,64},
H.J. Li¹⁹, H.N. Li^{56,j}, Hui Li⁴³, J.R. Li⁶¹, J.S. Li⁵⁹, K. Li¹, K.L. Li¹⁹, L.J. Li^{1,64}, Lei Li⁴⁸, M.H. Li⁴³,
P.L. Li⁶⁴, P.R. Li^{38,k,l}, Q.M. Li^{1,64}, Q.X. Li⁵⁰, R. Li^{17,31}, T. Li⁵⁰, T.Y. Li⁴³, W.D. Li^{1,64}, W.G. Li^{1,a},
X. Li^{1,64}, X.H. Li^{72,58}, X.L. Li⁵⁰, X.Y. Li^{1,8}, X.Z. Li⁵⁹, Y. Li¹⁹, Y.G. Li^{46,h}, Z.J. Li⁵⁹, Z.Y. Li⁷⁹,
C. Liang⁴², H. Liang^{72,58}, Y.F. Liang⁵⁴, Y.T. Liang^{31,64}, G.R. Liao¹⁴, Y.P. Liao^{1,64}, J. Libby²⁶,
A. Limphirat⁶⁰, C.C. Lin⁵⁵, C.X. Lin⁶⁴, D.X. Lin^{31,64}, T. Lin¹, B.J. Liu¹, B.X. Liu⁷⁷, C. Liu³⁴,
C.X. Liu¹, F. Liu¹, F.H. Liu⁵³, Feng Liu⁶, G.M. Liu^{56,j}, H. Liu^{38,k,l}, H.B. Liu¹⁵, H.H. Liu¹,
H.M. Liu^{1,64}, Huihui Liu²¹, J.B. Liu^{72,58}, K. Liu^{38,k,l}, K.Y. Liu⁴⁰, Ke Liu²², L. Liu^{72,58}, L.C. Liu⁴³,
Lu Liu⁴³, M.H. Liu^{12,g}, P.L. Liu¹, Q. Liu⁶⁴, S.B. Liu^{72,58}, T. Liu^{12,g}, W.K. Liu⁴³, W.M. Liu^{72,58},
X. Liu^{38,k,l}, X. Liu³⁹, Y. Liu^{38,k,l}, Y. Liu⁸¹, Y.B. Liu⁴³, Z.A. Liu^{1,58,64}, Z.D. Liu⁹, Z.Q. Liu⁵⁰,
X.C. Lou^{1,58,64}, F.X. Lu⁵⁹, H.J. Lu²³, J.G. Lu^{1,58}, Y. Lu⁷, Y.P. Lu^{1,58}, Z.H. Lu^{1,64}, C.L. Luo⁴¹,

J.R. Luo⁵⁹, M.X. Luo⁸⁰, T. Luo^{12,g}, X.L. Luo^{1,58}, X.R. Lyu⁶⁴, Y.F. Lyu⁴³, F.C. Ma⁴⁰, H. Ma⁷⁹, H.L. Ma¹, J.L. Ma^{1,64}, L.L. Ma⁵⁰, L.R. Ma⁶⁷, Q.M. Ma¹, R.Q. Ma^{1,64}, R.Y. Ma¹⁹, T. Ma^{72,58}, X.T. Ma^{1,64}, X.Y. Ma^{1,58}, Y.M. Ma³¹, F.E. Maas¹⁸, I. MacKay⁷⁰, M. Maggiora^{75A,75C}, S. Malde⁷⁰, Y.J. Mao^{46,h}, Z.P. Mao¹, S. Marcello^{75A,75C}, Y.H. Meng⁶⁴, Z.X. Meng⁶⁷, J.G. Messchendorp^{13,65}, G. Mezzadri^{29A}, H. Miao^{1,64}, T.J. Min⁴², R.E. Mitchell²⁷, X.H. Mo^{1,58,64}, B. Moses²⁷, N. Yu. Muchnoi^{4,c}, J. Muskalla³⁵, Y. Nefedov³⁶, F. Nerling^{18,e}, L.S. Nie²⁰, I.B. Nikolaev^{4,c}, Z. Ning^{1,58}, S. Nisar^{11,m}, Q.L. Niu^{38,k,l}, W.D. Niu⁵⁵, Y. Niu⁵⁰, S.L. Olsen^{10,64}, Q. Ouyang^{1,58,64}, S. Pacetti^{28B,28C}, X. Pan⁵⁵, Y. Pan⁵⁷, A. Pathak¹⁰, Y.P. Pei^{72,58}, M. Pelizaes³, H.P. Peng^{72,58}, Y.Y. Peng^{38,k,l}, K. Peters^{13,e}, J.L. Ping⁴¹, R.G. Ping^{1,64}, S. Plura³⁵, V. Prasad³³, F.Z. Qi¹, H.R. Qi⁶¹, M. Qi⁴², S. Qian^{1,58}, W.B. Qian⁶⁴, C.F. Qiao⁶⁴, J.H. Qiao¹⁹, J.J. Qin⁷³, L.Q. Qin¹⁴, L.Y. Qin^{72,58}, X.P. Qin^{12,g}, X.S. Qin⁵⁰, Z.H. Qin^{1,58}, J.F. Qiu¹, Z.H. Qu⁷³, C.F. Redmer³⁵, K.J. Ren³⁹, A. Rivetti^{75C}, M. Rolo^{75C}, G. Rong^{1,64}, Ch. Rosner¹⁸, M.Q. Ruan^{1,58}, S.N. Ruan⁴³, N. Salone⁴⁴, A. Sarantsev^{36,d}, Y. Schelhaas³⁵, K. Schoenning⁷⁶, M. Scodreggio^{29A}, K.Y. Shan^{12,g}, W. Shan²⁴, X.Y. Shan^{72,58}, Z.J. Shang^{38,k,l}, J.F. Shangguan¹⁶, L.G. Shao^{1,64}, M. Shao^{72,58}, C.P. Shen^{12,g}, H.F. Shen^{1,8}, W.H. Shen⁶⁴, X.Y. Shen^{1,64}, B.A. Shi⁶⁴, H. Shi^{72,58}, J.L. Shi^{12,g}, J.Y. Shi¹, S.Y. Shi⁷³, X. Shi^{1,58}, J.J. Song¹⁹, T.Z. Song⁵⁹, W.M. Song^{34,1}, Y.J. Song^{12,g}, Y.X. Song^{46,h,n}, S. Sosio^{75A,75C}, S. Spataro^{75A,75C}, F. Stieler³⁵, S. S. Su⁴⁰, Y.J. Su⁶⁴, G.B. Sun⁷⁷, G.X. Sun¹, H. Sun⁶⁴, H.K. Sun¹, J.F. Sun¹⁹, K. Sun⁶¹, L. Sun⁷⁷, S.S. Sun^{1,64}, T. Sun^{51,f}, Y.J. Sun^{72,58}, Y.Z. Sun¹, Z.Q. Sun^{1,64}, Z.T. Sun⁵⁰, C.J. Tang⁵⁴, G.Y. Tang¹, J. Tang⁵⁹, M. Tang^{72,58}, Y.A. Tang⁷⁷, L.Y. Tao⁷³, M. Tat⁷⁰, J.X. Teng^{72,58}, V. Thoren⁷⁶, W.H. Tian⁵⁹, Y. Tian^{31,64}, Z.F. Tian⁷⁷, I. Uman^{62B}, Y. Wan⁵⁵, S.J. Wang⁵⁰, B. Wang¹, Bo Wang^{72,58}, C. Wang¹⁹, D.Y. Wang^{46,h}, H.J. Wang^{38,k,l}, J.J. Wang⁷⁷, J.P. Wang⁵⁰, K. Wang^{1,58}, L.L. Wang¹, L.W. Wang³⁴, M. Wang⁵⁰, N.Y. Wang⁶⁴, S. Wang^{38,k,l}, S. Wang^{12,g}, T. Wang^{12,g}, T.J. Wang⁴³, W. Wang⁵⁹, W. Wang⁷³, W.P. Wang^{35,58,72,o}, X. Wang^{46,h}, X.F. Wang^{38,k,l}, X.J. Wang³⁹, X.L. Wang^{12,g}, X.N. Wang¹, Y. Wang⁶¹, Y.D. Wang⁴⁵, Y.F. Wang^{1,58,64}, Y.H. Wang^{38,k,l}, Y.L. Wang¹⁹, Y.N. Wang⁴⁵, Y.Q. Wang¹, Yaqian Wang¹⁷, Yi Wang⁶¹, Z. Wang^{1,58}, Z.L. Wang⁷³, Z.Y. Wang^{1,64}, D.H. Wei¹⁴, F. Weidner⁶⁹, S.P. Wen¹, Y.R. Wen³⁹, U. Wiedner³, G. Wilkinson⁷⁰, M. Wolke⁷⁶, L. Wollenberg³, C. Wu³⁹, J.F. Wu^{1,8}, L.H. Wu¹, L.J. Wu^{1,64}, Lianjie Wu¹⁹, X. Wu^{12,g}, X.H. Wu³⁴, Y.H. Wu⁵⁵, Y.J. Wu³¹, Z. Wu^{1,58}, L. Xia^{72,58}, X.M. Xian³⁹, B.H. Xiang^{1,64}, T. Xiang^{46,h}, D. Xiao^{38,k,l}, G.Y. Xiao⁴², H. Xiao⁷³, Y.L. Xiao^{12,g}, Z.J. Xiao⁴¹, C. Xie⁴², X.H. Xie^{46,h}, Y. Xie⁵⁰, Y.G. Xie^{1,58}, Y.H. Xie⁶, Z.P. Xie^{72,58}, T.Y. Xing^{1,64}, C.F. Xu^{1,64}, C.J. Xu⁵⁹, G.F. Xu¹, M. Xu^{72,58}, Q.J. Xu¹⁶, Q.N. Xu³⁰, W.L. Xu⁶⁷, X.P. Xu⁵⁵, Y. Xu⁴⁰, Y.C. Xu⁷⁸, Z.S. Xu⁶⁴, F. Yan^{12,g}, L. Yan^{12,g}, W.B. Yan^{72,58}, W.C. Yan⁸¹, W.P. Yan¹⁹, X.Q. Yan^{1,64}, H.J. Yang^{51,f}, H.L. Yang³⁴, H.X. Yang¹, J.H. Yang⁴², R.J. Yang¹⁹, T. Yang¹, Y. Yang^{12,g}, Y.F. Yang⁴³, Y.X. Yang^{1,64}, Y.Z. Yang¹⁹, Z.W. Yang^{38,k,l}, Z.P. Yao⁵⁰, M. Ye^{1,58}, M.H. Ye⁸, Junhao Yin⁴³, Z.Y. You⁵⁹, B.X. Yu^{1,58,64}, C.X. Yu⁴³, G. Yu¹³, J.S. Yu^{25,i}, M.C. Yu⁴⁰, T. Yu⁷³, X.D. Yu^{46,h}, C.Z. Yuan^{1,64}, J. Yuan³⁴, J. Yuan⁴⁵, L. Yuan², S.C. Yuan^{1,64}, Y. Yuan^{1,64}, Z.Y. Yuan⁵⁹, C.X. Yue³⁹, Ying Yue¹⁹, A.A. Zafar⁷⁴, F.R. Zeng⁵⁰, S.H. Zeng⁶³, X. Zeng^{12,g}, Y. Zeng^{25,i}, Y.J. Zeng⁵⁹, Y.J. Zeng^{1,64}, X.Y. Zhai³⁴, Y.C. Zhai⁵⁰, Y.H. Zhan⁵⁹, A.Q. Zhang^{1,64}, B.L. Zhang^{1,64}, B.X. Zhang¹, D.H. Zhang⁴³, G.Y. Zhang¹⁹, H. Zhang^{72,58}, H. Zhang⁸¹, H.C. Zhang^{1,58,64}, H.H. Zhang⁵⁹, H.Q. Zhang^{1,58,64}, H.R. Zhang^{72,58}, H.Y. Zhang^{1,58}, J. Zhang⁵⁹, J. Zhang⁸¹, J.J. Zhang⁵², J.L. Zhang²⁰, J.Q. Zhang⁴¹, J.S. Zhang^{12,g}, J.W. Zhang^{1,58,64}, J.X. Zhang^{38,k,l}, J.Y. Zhang¹, J.Z. Zhang^{1,64}, Jianyu Zhang⁶⁴, L.M. Zhang⁶¹, Lei Zhang⁴², P. Zhang^{1,64}, Q. Zhang¹⁹, Q.Y. Zhang³⁴, R.Y. Zhang^{38,k,l}, S.H. Zhang^{1,64}, Shulei Zhang^{25,i},

X.M. Zhang¹, X. Y Zhang⁴⁰, X.Y. Zhang⁵⁰, Y. Zhang¹, Y. Zhang⁷³, Y.T. Zhang⁸¹, Y.H. Zhang^{1,58}, Y.M. Zhang³⁹, Yan Zhang^{72,58}, Z.D. Zhang¹, Z.H. Zhang¹, Z.L. Zhang³⁴, Z.X. Zhang¹⁹, Z.Y. Zhang⁴³, Z.Y. Zhang⁷⁷, Z.Z. Zhang⁴⁵, Zh. Zh. Zhang¹⁹, G. Zhao¹, J.Y. Zhao^{1,64}, J.Z. Zhao^{1,58}, L. Zhao¹, Lei Zhao^{72,58}, M.G. Zhao⁴³, N. Zhao⁷⁹, R.P. Zhao⁶⁴, S.J. Zhao⁸¹, Y.B. Zhao^{1,58}, Y.X. Zhao^{31,64}, Z.G. Zhao^{72,58}, A. Zhemchugov^{36,b}, B. Zheng⁷³, B.M. Zheng³⁴, J.P. Zheng^{1,58}, W.J. Zheng^{1,64}, X.R. Zheng¹⁹, Y.H. Zheng⁶⁴, B. Zhong⁴¹, X. Zhong⁵⁹, H. Zhou^{35,50,o}, J.Y. Zhou³⁴, S. Zhou⁶, X. Zhou⁷⁷, X.K. Zhou⁶, X.R. Zhou^{72,58}, X.Y. Zhou³⁹, Y.Z. Zhou^{12,g}, Z.C. Zhou²⁰, A.N. Zhu⁶⁴, J. Zhu⁴³, K. Zhu¹, K.J. Zhu^{1,58,64}, K.S. Zhu^{12,g}, L. Zhu³⁴, L.X. Zhu⁶⁴, S.H. Zhu⁷¹, T.J. Zhu^{12,g}, W.D. Zhu⁴¹, W.J. Zhu¹, W.Z. Zhu¹⁹, Y.C. Zhu^{72,58}, Z.A. Zhu^{1,64}, J.H. Zou¹, J. Zu^{72,58}

¹ *Institute of High Energy Physics, Beijing 100049, People's Republic of China*

² *Beihang University, Beijing 100191, People's Republic of China*

³ *Bochum Ruhr-University, D-44780 Bochum, Germany*

⁴ *Budker Institute of Nuclear Physics SB RAS (BINP), Novosibirsk 630090, Russia*

⁵ *Carnegie Mellon University, Pittsburgh, Pennsylvania 15213, U.S.A.*

⁶ *Central China Normal University, Wuhan 430079, People's Republic of China*

⁷ *Central South University, Changsha 410083, People's Republic of China*

⁸ *China Center of Advanced Science and Technology, Beijing 100190, People's Republic of China*

⁹ *China University of Geosciences, Wuhan 430074, People's Republic of China*

¹⁰ *Chung-Ang University, Seoul, 06974, Republic of Korea*

¹¹ *COMSATS University Islamabad, Lahore Campus, Defence Road, Off Raiwind Road, 54000 Lahore, Pakistan*

¹² *Fudan University, Shanghai 200433, People's Republic of China*

¹³ *GSI Helmholtzcentre for Heavy Ion Research GmbH, D-64291 Darmstadt, Germany*

¹⁴ *Guangxi Normal University, Guilin 541004, People's Republic of China*

¹⁵ *Guangxi University, Nanning 530004, People's Republic of China*

¹⁶ *Hangzhou Normal University, Hangzhou 310036, People's Republic of China*

¹⁷ *Hebei University, Baoding 071002, People's Republic of China*

¹⁸ *Helmholtz Institute Mainz, Staudinger Weg 18, D-55099 Mainz, Germany*

¹⁹ *Henan Normal University, Xinxiang 453007, People's Republic of China*

²⁰ *Henan University, Kaifeng 475004, People's Republic of China*

²¹ *Henan University of Science and Technology, Luoyang 471003, People's Republic of China*

²² *Henan University of Technology, Zhengzhou 450001, People's Republic of China*

²³ *Huangshan College, Huangshan 245000, People's Republic of China*

²⁴ *Hunan Normal University, Changsha 410081, People's Republic of China*

²⁵ *Hunan University, Changsha 410082, People's Republic of China*

²⁶ *Indian Institute of Technology Madras, Chennai 600036, India*

²⁷ *Indiana University, Bloomington, Indiana 47405, U.S.A.*

²⁸ *INFN Laboratori Nazionali di Frascati, (A)INFN Laboratori Nazionali di Frascati, I-00044, Frascati, Italy; (B)INFN Sezione di Perugia, I-06100, Perugia, Italy; (C)University of Perugia, I-06100, Perugia, Italy*

²⁹ *INFN Sezione di Ferrara, (A)INFN Sezione di Ferrara, I-44122, Ferrara, Italy; (B)University of Ferrara, I-44122, Ferrara, Italy*

³⁰ *Inner Mongolia University, Hohhot 010021, People's Republic of China*

³¹ *Institute of Modern Physics, Lanzhou 730000, People's Republic of China*

³² *Institute of Physics and Technology, Peace Avenue 54B, Ulaanbaatar 13330, Mongolia*

³³ *Instituto de Alta Investigación, Universidad de Tarapacá, Casilla 7D, Arica 1000000, Chile*

³⁴ *Jilin University, Changchun 130012, People's Republic of China*

³⁵ *Johannes Gutenberg University of Mainz, Johann-Joachim-Becher-Weg 45, D-55099 Mainz, Germany*

³⁶ *Joint Institute for Nuclear Research, 141980 Dubna, Moscow region, Russia*

³⁷ *Justus-Liebig-Universität Giessen, II. Physikalisches Institut, Heinrich-Buff-Ring 16, D-35392 Giessen, Germany*

- ³⁸ Lanzhou University, Lanzhou 730000, People's Republic of China
- ³⁹ Liaoning Normal University, Dalian 116029, People's Republic of China
- ⁴⁰ Liaoning University, Shenyang 110036, People's Republic of China
- ⁴¹ Nanjing Normal University, Nanjing 210023, People's Republic of China
- ⁴² Nanjing University, Nanjing 210093, People's Republic of China
- ⁴³ Nankai University, Tianjin 300071, People's Republic of China
- ⁴⁴ National Centre for Nuclear Research, Warsaw 02-093, Poland
- ⁴⁵ North China Electric Power University, Beijing 102206, People's Republic of China
- ⁴⁶ Peking University, Beijing 100871, People's Republic of China
- ⁴⁷ Qufu Normal University, Qufu 273165, People's Republic of China
- ⁴⁸ Renmin University of China, Beijing 100872, People's Republic of China
- ⁴⁹ Shandong Normal University, Jinan 250014, People's Republic of China
- ⁵⁰ Shandong University, Jinan 250100, People's Republic of China
- ⁵¹ Shanghai Jiao Tong University, Shanghai 200240, People's Republic of China
- ⁵² Shanxi Normal University, Linfen 041004, People's Republic of China
- ⁵³ Shanxi University, Taiyuan 030006, People's Republic of China
- ⁵⁴ Sichuan University, Chengdu 610064, People's Republic of China
- ⁵⁵ Soochow University, Suzhou 215006, People's Republic of China
- ⁵⁶ South China Normal University, Guangzhou 510006, People's Republic of China
- ⁵⁷ Southeast University, Nanjing 211100, People's Republic of China
- ⁵⁸ State Key Laboratory of Particle Detection and Electronics, Beijing 100049, Hefei 230026, People's Republic of China
- ⁵⁹ Sun Yat-Sen University, Guangzhou 510275, People's Republic of China
- ⁶⁰ Suranaree University of Technology, University Avenue 111, Nakhon Ratchasima 30000, Thailand
- ⁶¹ Tsinghua University, Beijing 100084, People's Republic of China
- ⁶² Turkish Accelerator Center Particle Factory Group, (A)Istinye University, 34010, Istanbul, Turkey; (B)Near East University, Nicosia, North Cyprus, 99138, Mersin 10, Turkey
- ⁶³ University of Bristol, H H Wills Physics Laboratory, Tyndall Avenue, Bristol, BS8 1TL, U.K.
- ⁶⁴ University of Chinese Academy of Sciences, Beijing 100049, People's Republic of China
- ⁶⁵ University of Groningen, NL-9747 AA Groningen, The Netherlands
- ⁶⁶ University of Hawaii, Honolulu, Hawaii 96822, U.S.A.
- ⁶⁷ University of Jinan, Jinan 250022, People's Republic of China
- ⁶⁸ University of Manchester, Oxford Road, Manchester, M13 9PL, United Kingdom
- ⁶⁹ University of Muenster, Wilhelm-Klemm-Strasse 9, 48149 Muenster, Germany
- ⁷⁰ University of Oxford, Keble Road, Oxford OX13RH, United Kingdom
- ⁷¹ University of Science and Technology Liaoning, Anshan 114051, People's Republic of China
- ⁷² University of Science and Technology of China, Hefei 230026, People's Republic of China
- ⁷³ University of South China, Hengyang 421001, People's Republic of China
- ⁷⁴ University of the Punjab, Lahore-54590, Pakistan
- ⁷⁵ University of Turin and INFN, (A)University of Turin, I-10125, Turin, Italy; (B)University of Eastern Piedmont, I-15121, Alessandria, Italy; (C)INFN, I-10125, Turin, Italy
- ⁷⁶ Uppsala University, Box 516, SE-75120 Uppsala, Sweden
- ⁷⁷ Wuhan University, Wuhan 430072, People's Republic of China
- ⁷⁸ Yantai University, Yantai 264005, People's Republic of China
- ⁷⁹ Yunnan University, Kunming 650500, People's Republic of China
- ⁸⁰ Zhejiang University, Hangzhou 310027, People's Republic of China
- ⁸¹ Zhengzhou University, Zhengzhou 450001, People's Republic of China

^a Deceased

^b Also at the Moscow Institute of Physics and Technology, Moscow 141700, Russia

^c Also at the Novosibirsk State University, Novosibirsk, 630090, Russia

^d Also at the NRC "Kurchatov Institute", PNPI, 188300, Gatchina, Russia

^e Also at Goethe University Frankfurt, 60323 Frankfurt am Main, Germany

^f Also at Key Laboratory for Particle Physics, Astrophysics and Cosmology, Ministry of Education; Shanghai Key Laboratory for Particle Physics and Cosmology; Institute of Nuclear and Particle Physics, Shanghai 200240, People's Republic of China

^g Also at Key Laboratory of Nuclear Physics and Ion-beam Application (MOE) and Institute of Modern Physics, Fudan University, Shanghai 200443, People's Republic of China

^h Also at State Key Laboratory of Nuclear Physics and Technology, Peking University, Beijing 100871, People's Republic of China

ⁱ Also at School of Physics and Electronics, Hunan University, Changsha 410082, China

^j Also at Guangdong Provincial Key Laboratory of Nuclear Science, Institute of Quantum Matter, South China Normal University, Guangzhou 510006, China

^k Also at MOE Frontiers Science Center for Rare Isotopes, Lanzhou University, Lanzhou 730000, People's Republic of China

^l Also at Lanzhou Center for Theoretical Physics, Lanzhou University, Lanzhou 730000, People's Republic of China

^m Also at the Department of Mathematical Sciences, IBA, Karachi 75270, Pakistan

ⁿ Also at Ecole Polytechnique Federale de Lausanne (EPFL), CH-1015 Lausanne, Switzerland

^o Also at Helmholtz Institute Mainz, Staudinger Weg 18, D-55099 Mainz, Germany